



# Lawrence Berkeley Laboratory

UNIVERSITY OF CALIFORNIA

Submitted to Physical Review C

TARGET FRAGMENT ENERGIES AND MOMENTA IN THE REACTION  
OF 4.8 GeV  $^{12}\text{C}$  AND 5.0 GeV  $^{20}\text{Ne}$  WITH  $^{238}\text{U}$

W. Loveland, Cheng Luo, P. L. McGaughey, D. J. Morrissey  
and G. T. Seaborg

October 1980

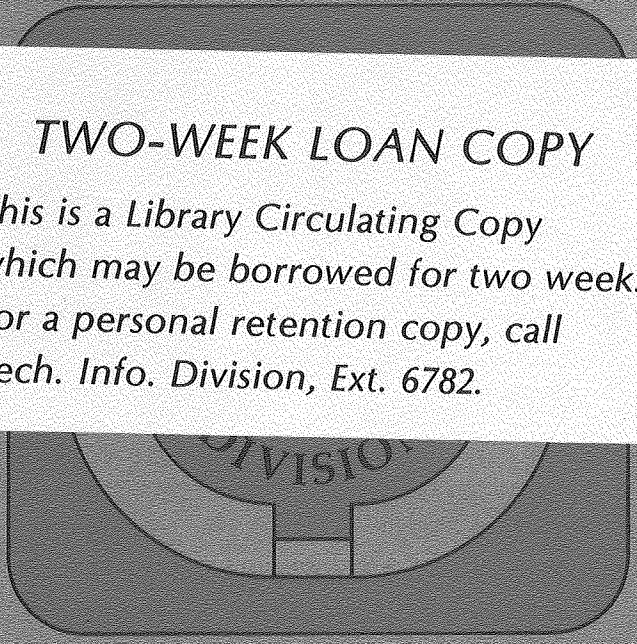
RECEIVED  
LAWRENCE  
BERKELEY LABORATORY

NOV 20 1980

LIBRARY AND  
DOCUMENTS SECTION

## TWO-WEEK LOAN COPY

*This is a Library Circulating Copy  
which may be borrowed for two weeks.  
For a personal retention copy, call  
Tech. Info. Division, Ext. 6782.*



LBL-11658 c. 2

## DISCLAIMER

This document was prepared as an account of work sponsored by the United States Government. While this document is believed to contain correct information, neither the United States Government nor any agency thereof, nor the Regents of the University of California, nor any of their employees, makes any warranty, express or implied, or assumes any legal responsibility for the accuracy, completeness, or usefulness of any information, apparatus, product, or process disclosed, or represents that its use would not infringe privately owned rights. Reference herein to any specific commercial product, process, or service by its trade name, trademark, manufacturer, or otherwise, does not necessarily constitute or imply its endorsement, recommendation, or favoring by the United States Government or any agency thereof, or the Regents of the University of California. The views and opinions of authors expressed herein do not necessarily state or reflect those of the United States Government or any agency thereof or the Regents of the University of California.

TARGET FRAGMENT ENERGIES AND MOMENTA IN THE REACTION  
OF 4.8 GeV  $^{12}\text{C}$  and 5.0 GeV  $^{20}\text{Ne}$  WITH  $^{238}\text{U}$

W. Loveland and Cheng Luo<sup>†</sup>  
Department of Chemistry, Oregon State University  
Corvallis, Oregon 97551

P. L. McGaughey, D. J. Morrissey and G. T. Seaborg  
Nuclear Science Division, Lawrence Berkeley Laboratory  
and Department of Chemistry  
University of California  
Berkeley, California 94720

ABSTRACT

Target fragment recoil properties were measured using the thick target-thick catcher technique for the interaction of 4.8 GeV  $^{12}\text{C}$  and 5.0 GeV  $^{20}\text{Ne}$  with  $^{238}\text{U}$ . The target fragment energies and momenta are very similar for the reaction of 4.8 GeV (400 MeV/A)  $^{12}\text{C}$  and 5.0 GeV (250 MeV/A)  $^{20}\text{Ne}$  with  $^{238}\text{U}$ . In the complex variation of fragment momenta with their N/Z ratio, one finds evidence suggesting the existence of several mechanisms leading to the formation of the target fragments. Comparison of these results with the predictions of the intranuclear cascade model of Yariv and Fraenkel and the firestreak model shows that both model predictions grossly overestimate the target fragment momenta.

NUCLEAR REACTIONS:  $^{238}\text{U}(^{12}\text{C},\text{X})$ ,  $E = 4.8$  GeV;  $^{238}\text{U}$   
 $(^{20}\text{Ne},\text{X})$ ,  $E = 5.0$  GeV; measured target fragment recoil  
properties; deduced target fragment energies, momenta;  
relativistic heavy ion reactions; target fragmentation;  
spallation; fission; intranuclear cascade model; firestreak  
model; thick target-thick catcher technique; Ge(Li) gamma-ray  
spectroscopy.

## I. INTRODUCTION

The study of the fragmentation of a  $^{238}\text{U}$  target nucleus induced by relativistic heavy ion (RHI) projectiles has from the outset revealed many new and interesting phenomena. In the first measurements of the yields of target fragments of differing  $Z$  and  $A$  from the reaction of 25.2 GeV  $^{12}\text{C}$  with  $^{238}\text{U}$ , Loveland et al<sup>1</sup> found, in addition to the expected yields of fission fragments, surprisingly large yields of fragments with  $160 \leq A \leq 190$  (see Figure 1). Subsequent measurements by McGaughey et al<sup>2</sup> for the reaction of 8.0 GeV  $^{20}\text{Ne}$  with  $^{238}\text{U}$  showed a smaller enhancement of these heavy product yields (see Figure 1), but the yields of these products still appeared to exceed any such yields observed in the reaction of protons with  $^{238}\text{U}$ . Spurred by these observations, Jacak and co-workers<sup>3</sup> extended the previous measurements<sup>4,5</sup> of target fragment yields in the reaction of 28 GeV protons with  $^{238}\text{U}$  beyond mass number 160 to see if any evidence could be found for such yields in proton-induced reactions. A small group of enhanced product yields were found for  $185 \leq A \leq 200$ ! (See Figure 1.) Comparison of the experimental yield distributions with the yield distributions calculated using the abrasion-ablation model<sup>6</sup>, the intranuclear cascade model of Yariv and Fraenkel<sup>7</sup> and the firestreak model<sup>8</sup> demonstrated that these fragments could be understood as being the survivors of a deep spallation process (involving significant projectile-target overlap) that resulted in the removal of as many as 80 nucleons from the target nucleus. These studies of target fragmentation involving  $^{238}\text{U}$  target nuclei

appear to show features, [i.e., the variation of yield distributions with projectile energy (violation of "limiting fragmentation") and the general non-equivalence of product distributions from RHI- and proton-induced reactions (violation of "factorization")] not seen in the interaction of RHI's with lighter targets<sup>9,10,11</sup>. (Small deviations from limiting fragmentation and factorization were observed for light products from the reaction of 25.2 GeV  $^{12}\text{C}$  with  $\text{Cu}^{12}$  and  $\text{Ag}^{13}$ .)

One of the most interesting questions to be addressed in the study of target fragmentation in relativistic nucleus-nucleus collisions is the mechanism(s) of energy transfer between projectile and target. Do the nucleons in the projectile and target interact as individual particles or is there a collective character to the interaction? At what value, if any, of the transferred energy does "saturation" take place? These and many similar questions are important components of the attempt to use relativistic nucleus-nucleus collisions to create new and unusual conditions in nuclear matter such as shock waves or to use these reactions to produce new nuclear species. The most sensitive experimental method for studying this transfer is to measure the target fragment kinematic properties (ie, their energies, momenta, and angular distributions). In support of this idea, we note that in the reaction of 8.0 GeV  $^{20}\text{Ne}$  with Ta, a consortium of investigators from ANL, BNL and LBL/OSU found<sup>14</sup> that the target fragment kinematic properties differed from those observed in the reaction of 25 GeV  $^{12}\text{C}$  or relativistic protons with heavy targets despite the fact that limiting fragmentation with respect to product yields, was observed<sup>11</sup>. The measurement of

target fragment momenta and energies can be more indicative of primary reaction processes than the measurement of target fragment yields because in the former measurements the effect of primary reaction processes and secondary processes involving de-excitation of the excited primary fragments can be unraveled<sup>15</sup>.

In this paper, we report the results of measurements of target fragment kinematic properties, using the thick target-thick catcher technique, for the reaction of 4.8 GeV (0.4 GeV/A)  $^{12}\text{C}$  and 5.0 GeV (0.250 GeV/A)  $^{20}\text{Ne}$  with  $^{238}\text{U}$ . In Section II, we discuss the experimental measurements and their analysis in terms of the two-step vector model of high energy reactions, while in Section III we discuss the results in detail comparing them to results of studies of relativistic proton-uranium collisions and current models of RHI reactions. In Section IV, we summarize the conclusion of our study.

## II. Experimental

Beams of 4.8 GeV  $^{12}\text{C}$  and 5.0 GeV  $^{20}\text{Ne}$  from the LBL Bevalac were used to irradiate a single thick depleted U foil ( $< 400$  ppm  $^{235}\text{U}$ ) of thickness 56.1 and 51.3 mg/cm<sup>2</sup>, respectively, surrounded by Mylar catcher foils of thickness 36 mg/cm<sup>2</sup>. The total particle fluences and irradiation lengths were  $6.19 \times 10^{13}$   $^{12}\text{C}/821.4$  min. and  $1.00 \times 10^{13}$   $^{20}\text{Ne}/639.8$  min., respectively. Assay of the radioactivities of the target fragments that stopped in the target, the forward and the backward catcher foils by  $\gamma$ -ray spectroscopy began approximately one hour after end of irradiation and measurements

continued for approximately six weeks. Standard techniques which have been described elsewhere<sup>16</sup> were used to identify the radionuclides present in each sample and to determine the activity of each nuclide in the forward, backward and target foils. No corrections were made to any of the activities for the effect of secondary induced reactions because previous studies<sup>17</sup> of p+U collisions using recoil techniques and targets five times thicker than those used in this work revealed such corrections to be < 5%. (The thicker targets used in the proton induced reaction studies should approximately compensate for the higher charged particle multiplicities observed in the RHI-induced reactions.)

The results of these measurements are presented as the fractions of each radionuclide which recoiled out of a target of thickness  $W$  ( $\text{mg}/\text{cm}^2$ ) in the forward and backward directions denoted by  $F$  and  $B$ , respectively. Tables I and II give a tabulation of the results for the forward-to-backward ratio,  $F/B$ , and a quantity approximately equal to the mean range of the recoil in the target material,  $2W(F+B)$  for the two reactions studied. Because of the complex variation of these quantities with the  $N/Z$  of the fragment, a simple plot of  $F/B$  or  $2W(F+B)$  vs.  $A$  would be a confusing jumble. Therefore we have chosen a set of common, mostly neutron-deficient nuclides for both data sets (indicated by the symbol \* in Table I) and have plotted the  $A$  dependence of  $F/B$  and  $2W(F+B)$  for the two reaction systems under study in Figures 2 and 3. The full complexity of the  $F/B$  values is shown in Figure 4 for the  $4.8 \text{ GeV } ^{12}\text{C} + ^{238}\text{U}$  reaction.

The results were transformed into kinematic quantities

using the two step vector model of high energy nuclear reactions, developed by Sugarman and co-workers.<sup>17-19</sup> The equations used in the analysis have been recently described by Winsberg.<sup>20</sup> In this model, the velocity,  $\vec{V}_\ell$ , of a recoil nuclide in the laboratory system is taken to be the sum of two vectors  $\vec{V}_\ell = \vec{v} + \vec{V}$ . The velocity vector  $\vec{v}$  results from the initial fast projectile-target interaction (the "abrasion" step of the abrasion-ablation model) while the velocity vector  $\vec{V}$ , assumed to be isotropic in the moving system, results from the slow de-excitation of the excited primary fragment (the "ablation step"). The vector  $\vec{v}$  is assumed to be constant while the values of the vector  $\vec{V}$  are assumed to have a Maxwellian distribution. No correlation is assumed to exist between the two vectors. The vector  $\vec{v}$  can be decomposed into its two orthogonal components parallel and perpendicular to the beam ( $v_\parallel$  and  $v_\perp$ ). In this analysis we have assumed  $v_\perp = 0$ . In converting product ranges into kinetic energies, we used the range-energy tables of Northcliffe and Schilling.<sup>21</sup> The results of this analysis are tabulated in Tables III and IV and are shown for the 4.8 GeV  $^{12}\text{C} + ^{238}\text{U}$  system in Figure 5. The validity of using this analysis for RHI-induced reactions is discussed in Ref. 14.

### III. Discussion of Results

One question of continuing interest concerning the mechanism(s) of energy transfer in relativistic nucleus-nucleus collisions is the question of whether the energy transfer scales as the total projectile kinetic energy or as the energy per nucleon of the projectile. It is of interest in this regard to

compare the target fragment kinematic properties for the reaction of 4.8 GeV  $^{12}\text{C}$  and 5.0 GeV  $^{20}\text{Ne}$  with  $^{238}\text{U}$  (approximately equivalent total projectile kinetic energy, considerably different energy per nucleon). By examining the data in Figures 2 and 3, one can see that, within experimental error, the target fragment kinematic properties for the two systems are generally similar with no obvious systematic differences between them. (There may be some hint of a difference in range for the heaviest products, but it is not demonstrated experimentally.) While these experimental data are necessary but not sufficient observations to establish the scaling of the energy transfer with total projectile kinetic energy, they probably do serve to justify the representation of the trends of both data sets by the discussion of the more complete, more precisely known data from the 4.8 GeV  $^{12}\text{C} + ^{238}\text{U}$  reaction. We shall adopt this viewpoint from this point forth. The observation of the equivalence of the two data sets is consistent with prior observations of Cumming et al<sup>9</sup> and Loveland et al<sup>11</sup> that the target fragment yields from RHI induced reactions most resemble the yields from reactions induced by protons of the same total projectile energy. This observation is also consistent with the data of Kaufman et al<sup>10</sup> who found that the target fragment recoil properties from the reaction of 25.2 GeV  $^{12}\text{C}$  with  $^{197}\text{Au}$  most resembled similar properties for the reaction of 28 GeV protons with Au.

In this regard, it is interesting to compare our results with similar results from the interaction of high energy protons with  $^{238}\text{U}$ . In Figures 2 and 3, we show a comparison between

the target fragment recoil properties for the reaction of 4.8 GeV  $^{12}\text{C}$  with  $^{238}\text{U}$  and similar measurements for the same products from the reaction of 450 MeV protons<sup>17</sup> and 3 GeV protons<sup>22,23,24</sup> with  $^{238}\text{U}$ . One is immediately struck by the fact that the non-fission F/B values for fragments from the RHI-induced reaction exceed any equivalent values for the proton-induced reactions. This trend is in accord with the data for the 8.0 GeV  $^{20}\text{Ne} + ^{181}\text{Ta}$  reaction and supports the conclusion of that study<sup>14</sup> that at these projectile energies (4.8 GeV  $^{12}\text{C}$ , 8.0 GeV  $^{20}\text{Ne}$ ) that limiting fragmentation has not been reached. The values of  $2W(F+B)$  are similar (within certain broad limits) for the products of the heavy ion and the proton-induced reactions. To understand the meaning of this latter observation, we compared the values of  $\langle P \rangle (= A \langle V \rangle)$  where  $P$  is the momentum of a nuclide with mass number  $A$  corresponding to the velocity  $V$ , for the nuclides considered in Figures 2 and 3.  $\langle P \rangle$  is the momentum imparted to the target fragments during the de-excitation step of the reaction. In examining this comparison, which is shown in Figure 6, one is struck by the general dependence of  $\langle P \rangle$  upon  $\sqrt{\Delta A}$ , the square root of the number of nucleons removed from the target, for the most neutron deficient species. (The solid curve represents exactly the same dependence of  $\langle P \rangle$  upon  $\sqrt{\Delta A}$  found<sup>14</sup> for the reaction of 8 GeV  $^{20}\text{Ne}$  with  $^{181}\text{Ta}$ . The dashed curve, which overlays the / dependence of  $\langle P \rangle$  upon  $\Delta A$  found for several deep spallation products in proton induced reactions<sup>34</sup>.) This dependence is indicative of sequential, step-wise momentum kicks being imparted to the fragment during the de-excitation phase of the reaction,

in accord with the basic assumptions of the two step vector model of high energy reactions. Those nuclei resulting primarily from the fission process, have much higher values of  $\langle P \rangle$  ( $> 2750$  MeV/c). The general equivalence of the  $\langle P \rangle$  values for the fragments produced in proton-induced deep spallation and by the interaction of  $4.8 \text{ GeV}^{12}\text{C}$  and  $8 \text{ GeV}^{20}\text{Ne}$  with heavy targets would argue that the de-excitation phase of these reactions is similar. This also implies that distributions (such as certain product yield distributions) which strongly reflect the de-excitation phase will show little dependence upon projectile energy or type.

Detailed examination of the data shown in Figures 4 and 5 shows the complexity of the target fragment kinematic properties in this reaction. In these Figures, we have plotted in contour plots the values of  $F/B$  and the target fragment kinetic energy  $\langle E \rangle$  as measured in a system moving with velocity  $v_{\parallel}$  as a function of the displacement of the fragment atomic number,  $Z$ , from the valley of  $\beta$ -stability,  $Z - Z_A$ .  $Z_A$  is the non-integral  $Z$  corresponding to the center of the valley<sup>29</sup> of  $\beta$ -stability for a given  $A$ . In Figure 5, one sees evidence for the occurrence of several different processes in the reaction of  $4.8 \text{ GeV}^{12}\text{C}$  with  $^{238}\text{U}$ . The lightest fragments ( $A < 40$ ) are characterized by high kinetic energies and large values of  $F/B$  which is consistent with their production in a "fragmentation" mechanism<sup>30</sup>. The heaviest fragments ( $A > 150$ ) are neutron-deficient, show very large values of  $F/B$  and very low fragment kinetic energies. Undoubtedly, these products are the result of deep spallation of  $^{238}\text{U}$  nuclei. The intermediate mass products ( $80 \leq A \leq 140$ ) are a

complex mixture of fission and deep spallation products. The most n-rich products ( $90 \leq A \leq 110$ ) are mostly fission fragments ( $F/B \sim 1$ , high kinetic energies). The mass and atomic numbers of these products and their kinetic energies are consistent with their formation in the fission of a species with  $A \sim 210$ ,  $Z \sim 85$  with some slight admixture of super-deep spallation products. Their kinetic energies are too low to be consistent with the fission of uranium-like species, a fact similar to that observed<sup>31</sup> in high energy photon-induced fission where fission occurs primarily at the end of the evaporation chains involved in de-excitation of the primary target fragments.

The group of fragments with  $40 \leq A \leq 70$  represents an interesting class of events. Their kinetic energies are relatively high and the values of  $F/B$  are also large ( $2 \leq F/B \leq 3$ ). One possible explanation of the origin of these events is that they represent the products of the fission of a species with  $A \sim 120-130$ . Their kinetic energies are completely consistent with this idea and their  $F/B$  ratios would indicate their formation in a non-peripheral collision. The other part of this scenario would be the large group of neutron-deficient products with  $120 \leq A \leq 130$  which represent the non-fissioning survivors of the precursors of the  $40 \leq A \leq 70$  events. Events of this character have been directly observed by Wilkins<sup>32</sup> et al and inferred by Chang and Sugarman<sup>33</sup> for the reaction of high energy protons with uranium.

An alternative explanation of the origin of the  $A=40-70$  fragments suggested by the intranuclear cascade model<sup>7</sup> and the firestreak model<sup>8</sup> is that these fragments are the result of the fission of species with  $A \sim 185$  that are highly excited

( $E^* \geq 1000$  MeV). The resulting fission fragments evaporate copious numbers of nucleons with  $A \sim 40-70$ .

To help our understanding of some of the empirical trends discussed above, we have compared our experimental results with two current models of relativistic heavy ion reactions, the intranuclear cascade model of Yariv and Fraenkel<sup>7</sup>, and a modified version of the firestreak model<sup>8,28</sup>. These models represent two extreme views of relativistic nuclear collisions, with the cascade model treating the projectile-target interaction as due to the uncorrelated collisions of individual particles in the projectile and target while the firestreak model assumes that all nucleons in the projectile-target overlap region interact collectively as part of the inelastic collision of two larger pieces of nuclear matter. A comparison of the results of calculations using these two models with experimental data might help to clarify the role of collective processes in energy transfer mechanism(s).

The collision of the RHI projectile with the target nucleus is treated as a two step process in the intranuclear cascade calculation, a fast step with cascading collisions of nucleons from one reaction partner inside the nucleus of the other partner, and a slow statistical evaporation step de-exciting the primary fragments after the fast cascading nucleons have escaped or have been captured by the primary fragments. The calculation is made using an extension of the intranuclear cascade code<sup>25</sup> (VEGAS) for proton-induced reactions which has been modified to treat two colliding nuclei<sup>7</sup>. The calculations were performed with step function

density distributions for both nuclei and without refraction and reflection of the cascading particles at the nuclear boundaries. Fermi motion was included in the projectile as well as in the target nucleus. An infinite rearrangement time was assumed for the nucleus to respond to the removal of nucleons from the Fermi sea by the fast cascade. Meson production and cascades were included via the ISOBAR model<sup>26</sup>. The impact parameter for each collision was selected at random, and the final production cross sections were integrated over impact parameter.

The de-excitation of the primary fragments from the fast cascade is calculated using a version of the Dostrovsky, Fraenkel and Friedlander statistical model calculations<sup>27,7</sup> which includes fission competition. The excitation energy, mass and atomic number of each fragment were obtained from the fast cascade calculation.

The modified firestreak model<sup>28</sup> is an extension of the fireball or abrasion-ablation model in which the assumption of interacting spherical nuclei with sharp surfaces making clean cuts through one another has been replaced by a more realistic assumption of interacting nuclei with diffuse surfaces due to the use of realistic nuclear density distributions<sup>8</sup>. The interaction between the colliding nuclei is assumed to be localized to the overlapping volume. In this region, colinear tubes of nuclear matter from the projectile and target undergo inelastic collisions with one another. (The probability of collision between the tubes is given by a transparency function based upon free nucleon-nucleon total reaction cross sections.) If the resulting kinetic energy of the collision product is less

than the binding energy of the nucleus, the tube is captured by the target residue and its energy, etc., contributes to the excitation energy, linear and angular momentum of the residue. Angular momentum is explicitly conserved in the interaction. De-excitation of the primary products is calculated using the same formalism as the cascade model.

In Figure 7, we show a comparison between the measured and calculated values of the longitudinal velocity  $\beta_{\parallel}$  ( $=v_{\parallel}/c$ ) imparted to the fragment in the first step of the projectile-target interaction for the 4.8 GeV  $^{12}\text{C} + ^{238}\text{U}$  reaction. The measured values of  $\beta_{\parallel}$  selected for use in Figure 7 are for neutron deficient species. This selection was made to emphasize deep spallation reactions and to de-emphasize fission, i.e. to select products from collisions with significant projectile-target overlap. As one can see from examining Figure 7, the cascade model grossly overestimates the values of  $\beta_{\parallel}$  for all fragments with  $A < 209$  with the firestreak model predictions also in gross disagreement with the experimental data. This situation may be analogous to the overestimates of the deep spallation product momenta in proton-nucleus collisions by cascade calculations<sup>34</sup>. Crespo, Cumming and Alexander<sup>34</sup> speculated that the primary spallation products might emit fragments such as  $^{24}\text{Na}$  thus reducing the spallation product momenta and providing a natural mechanism for producing the high momenta associated with these light fragments. This mechanism is not unreasonable given the calculated excitation energies (firestreak model) of the precursors of the  $A=160-190$  fragments which range in energy from 380 to 595 MeV, respectively. Also the values of  $\beta$  ( $\approx 0.006$ )

of the sources of the Na, etc. fragments emitted in p-U collisions<sup>35</sup> are supportive of this supposition because they are very similar to the calculated  $\beta$  values for the A=160-190 fragments. To help settle this question, it would be useful to measure the light fragment energies and masses in coincidence with deep spallation products from these reactions which have been identified as to energy and mass.

#### IV. Conclusions

What have we learned about target fragmentation in this work? The most important ideas supported by the data presented herein are as follows:

1. The transfer of energy, momentum, etc. to the target nucleus scales with the projectile total kinetic energy for relativistic nucleus-nucleus collisions occurring with projectiles of kinetic energy 250-400 MeV/A.

2. The relativistic nucleus-nucleus collision involves larger average transfer of forward momentum to the target fragments than seen in relativistic proton-induced reactions.

3. The momentum transfer for all but the most peripheral collisions may be either substantially less than predicted by current models of RHI interactions or the primary target fragments may emit light fragments which carry away substantial amounts of momentum.

4. There is evidence supportive of the existence of several different mechanisms in the reactions studied.

ACKNOWLEDGMENTS

This work was supported in part by the Nuclear Physics Division of the U.S. Department of Energy. We wish to thank Dr. S. B. Kaufman for allowing us to perform the 4.8 GeV  $^{12}\text{C}$  bombardment as a parasitic experiment with his irradiation. One of us (WDL) gratefully acknowledges financial support from the Lawrence Berkeley Laboratory during a portion of this work under U.S. Department of Energy contract W-7405-ENG-48.

REFERENCES

- + Permanent address: Atomic Energy Research Institute, Beijing, People's Republic of China.
1. W. Loveland, R. J. Otto, D. J. Morrissey, and G. T. Seaborg, Phys. Rev. Lett. 39, 320 (1977).
  2. P. L. McGaughey, W. Loveland, D. J. Morrissey, R. J. Otto and G. T. Seaborg, Oregon State University Report RLO-2227-TA35-M1, p. 27 (1979); P. L. McGaughey, D. J. Morrissey, W. Loveland, and G. T. Seaborg, Lawrence Berkeley Laboratory Report LBL-9711, p. 92 (1980).
  3. B. V. Jacak, D. J. Morrissey, M. Rodder, and G. T. Seaborg, Lawrence Berkeley Laboratory Report LBL-9711, p. 94 (1980).
  4. Y. Y. Chu, E. H. Franz, G. Friedlander and P. J. Karol, Phys. Rev. C4, 2202 (1971).
  5. Y. Y. Chu, G. Friedlander and L. Husain, Phys. Rev. C15, 352 (1977).
  6. See D. J. Morrissey, W. R. Marsh, R. J. Otto, W. Loveland, and G. T. Seaborg, Phys. Rev. C18, 1267 (1978) and references cited therein.
  7. Y. Yariv and Z. Fraenkel, Phys. Rev. C20, 2227, (1979).
  8. W. D. Myers, Nucl. Phys. A296, 117 (1978); J. Gosset, J. I. Kapusta, and G. D. Westfall, Phys. Rev. C18, 844 (1978).
  9. J. B. Cumming, R. W. Stoenner, and P. E. Haustein, Phys. Rev. C14, 1554 (1976); J. B. Cumming, P. E. Haustein, R. W. Stoenner, L. Mausner and R. A. Nausmann, Phys. Rev. C10, 739 (1974); J. B. Cumming, P. E. Haustein, T. J. Ruth, and G. J. Virtes, Phys. Rev. C17, 1632 (1978).
  10. S. B. Kaufman, E. P. Steinberg, and M. W. Weisfield, Phys. Rev. C18, 1349 (1978).
  11. P. L. McGaughey, L. L. Nunnolley, D. J. Morrissey, W. Loveland, and G. T. Seaborg, Oregon State University Report RLO-2227-TA35-M1, p. 62 (1979); W. Loveland, D. J. Morrissey, R. J. Otto and G. T. Seaborg, Lawrence Berkeley Laboratory Report LBL-10011 (1980).
  12. J. B. Cumming, P. E. Haustein and H. C. Hseuh, Phys. Rev. C18, 1372 (1978).

13. N. T. Porile, G. D. Cole and C. R. Rudy, Phys. Rev. C19, 2288 (1979).
14. W. Loveland, D. J. Morrissey, K. Aleklett, G. T. Seaborg, S. B. Kaufman, E. P. Steinberg, B. D. Wilkins, J. B. Cumming, P. E. Haustein, H. C. Hseuh, Lawrence Berkeley Laboratory Report LBL-10010 (1980); Phys. Rev. C (submitted for publication).
15. D. J. Morrissey, L. F. Oliveira, J. O. Rasmussen, G. T. Seaborg, Y. Yariv and Z. Fraenkel, Phys. Rev. Lett. 43, 1179 (1979).
16. D. J. Morrissey, D. Lee, R. J. Otto, and G. T. Seaborg, Nucl. Instr. Meth. 158, 499 (1978).
17. N. Sugarman, H. Munzel, J. A. Panontin, K. Wielgoz, M.V. Ramaniah, G. Lange, and E. Lopez-Mencherero, Phys. Rev. 143, 952 (1966).
18. N. T. Porile and N. Sugarman, Phys. Rev. 107, 1410 (1957).
19. N. Sugarman, M. Campos and K. Wielgoz, Phys. Rev. 101, 388 (1956).
20. L. Winsberg, Nucl. Instr. Meth. 150, 465 (1978).
21. L. C. Northcliffe and R. F. Schilling, Nucl. Data A7, 233 (1970).
22. V. P. Crespo, J. M. Alexander and E. K. Hyde, Phys. Rev. 131, 1765 (1963).
23. K. Beg and N. T. Porile, Phys. Rev. C3, 1631 (1971).
24. O. Scheidemann and N. T. Porile, Phys. Rev. C14, 1534 (1976).
25. K. Chen, Z. Fraenkel, G. Friedlander, J. R. Grover, J. M. Miller, and Y. Shimamoto, Phys. Rev. 166, 949 (1968).
26. G. D. Harp, K. Chen, G. Friedlander, Z. Fraenkel, and J. M. Miller, Phys. Rev. C8, 851 (1973).
27. I. Dostrovsky, Z. Fraenkel, and G. Friedlander, Phys. Rev. 116, 683 (1959).
28. The detailed extension of the firestreak model to describe target fragmentation is described in "Calculation of Target Residue Production with the Nuclear Firestreak Model", P.L. McGaughey, D.J. Morrissey, and G. T. Seaborg, 180th ACS National Meeting, San Francisco, CA, August, 1980.

29. A. H. Wapstra and K. Bos, At. Nucl. Data Tables 19, 177 (1977).
30. R. Wolfgang, E. W. Baker, A. A. Caretto, J. B. Cumming, G. Friedlander and J. Hudis, Phys. Rev. 103, 394 (1956).
31. K. Lindgren and G. G. Johsson, Nucl. Phys. A166, 643 (1971).
32. B. D. Wilkins, S. B. Kaufman, E. P. Steinberg, J. A. Urbon, and D. J. Henderson, Phys. Rev. Lett. 43, 1080 (1979).
33. S. K. Chang and N. Sugarman, Phys. Rev. C8, 775 (1973).
34. V.P. Crespo, J.B. Cumming and J.M. Alexander, Phys. Rev. C2, 1777 (1970).
35. G.D. Westfall, R.G. Sextro, A.M. Poskanzer, A.M. Zehelman, G.W. Butler, and E.K. Hyde, Phys. Rev. C17, 1368 (1978).

FIGURE CAPTIONS

- Figure 1. Isobaric yields of fragments produced in the interaction of relativistic projectiles with uranium. The data points are the measurements of Jacak *et al*<sup>3</sup> for the reaction of 28 GeV protons with uranium.
- Figure 2. Selected target fragment F/B values for the reactions of (a) 4.8 GeV  $^{12}\text{C}$  and (b) 5.0 GeV  $^{20}\text{Ne}$  with  $^{238}\text{U}$ .
- Figure 3. Selected target fragment  $2W(F+B)$  values ( $\approx$  range of the fragment in the target material) for the reactions of (a) 4.8 GeV  $^{12}\text{C}$  and (b) 5.0 GeV  $^{20}\text{Ne}$  with  $^{238}\text{U}$ .
- Figure 4. A contour plot of the fragment F/B values as a function of the fragment mass number A and its position relative to the center of the valley of  $\beta$ -stability ( $Z-Z_A$ ) for the reaction of 4.8 GeV  $^{12}\text{C}$  with  $^{238}\text{U}$ .
- Figure 5. A contour plot of the fragment kinetic energies  $\langle E \rangle$  as deduced in the two step vector model as a function of the fragment mass number A and its position relative to the center of the valley of  $\beta$ -stability,  $Z-Z_A$ , for the reaction of 4.8 GeV  $^{12}\text{C}$  with  $^{238}\text{U}$ .
- Figure 6. A comparison of the values of  $\langle P \rangle$ , the momentum imparted to selected target fragments in the reaction of 4.8 GeV  $^{12}\text{C}$  with  $^{238}\text{U}$ . See text for explanation of curves.
- Figure 7. A comparison of calculated and measured values of the target fragment longitudinal velocity component  $\beta_{\parallel}$  arising from the initial target-projectile interaction for the reaction of 4.8 GeV  $^{12}\text{C}$  with  $^{238}\text{U}$ .

Table I

Target Fragment Recoil Properties			
4.8 GeV $^{12}\text{C} + ^{238}\text{U}$			
Nuclide	$E_Y$ (keV)	F/B	2W(F+B)
* $^{24}\text{Na}$	1368.6	$5.5 \pm 0.8$	$20.3 \pm 2.6$
* $^{28}\text{Mg}$	400.6 941.7 1342.2 1778.9	$4.6 \pm 1.0$	$18.3 \pm 2.9$
* $^{43}\text{K}$	372.0 396.0 593.5	$4.7 \pm 1.0$	$14.6 \pm 3.0$
$^{44\text{m}}\text{Sc}$	270.9 1157.0	$3.2 \pm 0.4$	$10.9 \pm 1.0$
$^{46}\text{Sc}$	889.3 1120.5	$3.5 \pm 0.9$	$13.0 \pm 1.6$
* $^{48}\text{Sc}$	983.5 1037.6 1312.1	$2.9 \pm 0.5$	$10.0 \pm 1.2$
$^{48}\text{V}$	983.5 1311.6	$3.4 \pm 0.5$	$11.4 \pm 1.0$
$^{56}\text{Mn}$	846.6	$2.7 \pm 0.9$	$8.3 \pm 2.1$
$^{59}\text{Fe}$	1099.2 1291.6	$2.3 \pm 1.3$	$8.8 \pm 1.6$
$^{69\text{m}}\text{Zn}$	438.7	$1.8 \pm 0.2$	$11.0 \pm 1.1$
$^{71}\text{As}$	174.9	$2.6 \pm 0.4$	$9.5 \pm 1.4$
* $^{72}\text{As}$	834.0	$1.6 \pm 0.2$	$9.6 \pm 0.8$
$^{74}\text{As}$	595.9	$2.1 \pm 0.3$	$9.4 \pm 1.3$
* $^{76}\text{As}$	559.1	$2.2 \pm 0.3$	$8.1 \pm 0.8$
$^{77}\text{Br}$	520.7 579.4	$2.1 \pm 1.2$	$7.9 \pm 4.5$

Table I

Target Fragment Recoil Properties			
4.8 GeV $^{12}\text{C} + ^{238}\text{U}$			
Nuclide	$E_{\gamma}$ (keV)	F/B	2W(F+B)
$^{78}\text{As}$	694.9	$1.8 \pm 0.9$	$14.1 \pm 9.5$
$^{81}\text{Rb}$	190.4	$2.4 \pm 0.4$	$9.3 \pm 3.6$
$^{82}\text{Br}$	554.3	$1.2 \pm 0.3$	$6.6 \pm 1.0$
	689.4		
	827.8		
	1043.9		
	1317.4		
	1474.8		
$^{82\text{m}}\text{Rb}$	698.4	$2.1 \pm 0.7$	$6.7 \pm 2.3$
	827.6		
	1044.1		
	1317.5		
$^{83}\text{Rb}$	520.3	$1.9 \pm 0.7$	$8.1 \pm 1.5$
$^{86}\text{Rb}$	1078.8	$1.7 \pm 0.3$	$7.4 \pm 1.0$
$^{87\text{m}}\text{Y}$	381.1	$2.2 \pm 0.2$	$6.1 \pm 1.0$
$^{88}\text{Zr}$	392.8	$2.7 \pm 0.7$	$6.3 \pm 1.0$
$^{88}\text{Y}$	898.0	$2.1 \pm 0.2$	$9.3 \pm 2.8$
	1836.1		
* $^{89}\text{Zr}$	909.2	$2.2 \pm 0.3$	$7.5 \pm 0.6$
$^{90\text{m}}\text{Y}$	202.4	$1.7 \pm 0.3$	$8.0 \pm 0.9$
* $^{90}\text{Nb}$	1129.1	$2.6 \pm 0.6$	$5.6 \pm 0.9$
$^{91}\text{Sr}$	555.6	$1.3 \pm 0.2$	$11.0 \pm 1.4$
	652.9		
	749.8		
	925.8		
	1024.3		
$^{92}\text{Y}$	934.5	$1.2 \pm 0.3$	$7.9 \pm 1.5$

Table I

Target Fragment Recoil Properties 4.8 GeV $^{12}\text{C} + ^{238}\text{U}$			
Nuclide	$E_{\gamma}$ (keV)	F/B	2W(F+B)
$^{93\text{m}}\text{Mo}$	684.6	$2.0 \pm 1.8$	$5.8 \pm 1.8$
	1477.2		
$^{95}\text{Zr}$	724.2	$1.1 \pm 0.1$	$9.6 \pm 0.7$
	756.7		
$^{95}\text{Nb}$	765.8	$1.5 \pm 0.3$	$4.2 \pm 0.5$
$^{95}\text{Tc}$	765.8	$3.3 \pm 0.8$	$6.2 \pm 0.8$
* $^{96}\text{Nb}$	460.0	$1.3 \pm 0.3$	$7.6 \pm 1.1$
	568.9		
	849.9		
	1091.3		
	1200.2		
	1497.7		
* $^{96}\text{Tc}$	812.5	$2.2 \pm 0.3$	$6.5 \pm 0.6$
	849.9		
	1126.8		
$^{97}\text{Ru}$	215.7	$2.5 \pm 0.6$	$5.4 \pm 0.5$
* $^{97}\text{Zr}$	355.4	$1.2 \pm 0.2$	$9.8 \pm 2.0$
	743.4		
	1148.0		
	1750.5		
* $^{99}\text{Mo}$	140.5	$1.3 \pm 0.1$	$9.6 \pm 0.2$
	181.1		
	364.5		
	739.6		
$^{101\text{m}}\text{Rh}$	306.8	$2.4 \pm 1.0$	$5.9 \pm 1.3$
$^{103}\text{Ru}$	497.1	$1.4 \pm 0.2$	$9.3 \pm 0.9$
$^{105}\text{Ru}$	316.5	$1.1 \pm 0.2$	$9.8 \pm 1.5$
	469.4		
	676.3		
	724.2		

Table I

Target Fragment Recoil Properties			
4.8 GeV $^{12}\text{C} + ^{238}\text{U}$			
Nuclide	$E_{\gamma}$ (keV)	F/B	2W(F+B)
$^{105}\text{Rh}$	319.2	$1.9 \pm 0.3$	$7.9 \pm 0.7$
$^{106\text{m}}\text{Ag}$	406.0	$0.8 \pm 0.4$	$6.3 \pm 1.8$
	429.5		
	450.8		
	1199.1		
	1527.0		
$^{111}\text{In}$	150.6	$2.5 \pm 0.3$	$5.2 \pm 1.9$
	171.3		
	245.4		
$^{111\text{m}}\text{Pd}$	172.1	$1.5 \pm 0.4$	$10.7 \pm 2.2$
$^{115}\text{Cd}$	492.3	$1.3 \pm 0.4$	$9.4 \pm 1.9$
	527.9		
$^{115\text{m}}\text{In}$	336.3	$1.3 \pm 0.6$	$13.5 \pm 6.8$
$^{117\text{m}}\text{Sn}$	158.4	$1.7 \pm 1.1$	$9.0 \pm 6.2$
$^{117}\text{Sb}$	158.5	$1.5 \pm 0.4$	$5.4 \pm 1.6$
$^{119\text{m}}\text{Te}$	1136.0	$2.4 \pm 0.2$	$5.1 \pm 0.5$
	1212.7		
$^{120}\text{Sb}$	197.3	$1.7 \pm 0.2$	$4.5 \pm 0.6$
$^{121}\text{Te}$	573.1	$2.8 \pm 0.5$	$4.1 \pm 0.7$
$^{122}\text{Sb}$	563.9	$1.4 \pm 0.3$	$8.1 \pm 1.1$
$^{124}\text{Sb}$	602.7	$0.8 \pm 0.3$	$6.9 \pm 2.0$
	1691.0		
$^{124}\text{I}$	602.7	$1.8 \pm 0.4$	$6.5 \pm 0.8$
	1691.0		
$^{127}\text{Sb}$	252.7	$1.0 \pm 0.1$	$8.7 \pm 2.1$
	473.2		
	685.7		

Table I

Target Fragment Recoil Properties			
4.8 GeV $^{12}\text{C} + ^{238}\text{U}$			
Nuclide	$E_{\gamma}$ (keV)	F/B	2W(F+B)
$^{130}\text{I}$	448.0	$1.4 \pm 0.2$	$6.9 \pm 3.7$
	739.4		
	1157.3		
$^{131}\text{Ba}$	123.7	$2.6 \pm 0.3$	$4.4 \pm 0.3$
	216.0		
* $^{131}\text{I}$	364.5	$1.2 \pm 0.1$	$8.4 \pm 4.5$
	637.0		
$^{132}\text{Te}$	228.2	$1.1 \pm 0.1$	$7.1 \pm 0.6$
	667.7		
	954.6		
	1398.5		
$^{132}\text{Cs}$	667.7	$1.7 \pm 1.2$	$5.7 \pm 3.0$
$^{132}\text{I}$	667.7	$1.3 \pm 0.3$	$5.3 \pm 0.8$
	954.6		
* $^{133}\text{I}$	529.5	$1.1 \pm 0.2$	$8.8 \pm 0.9$
$^{135}\text{Xe}$	249.6	$1.2 \pm 0.2$	$8.2 \pm 0.9$
$^{135}\text{I}$	1038.8	$1.4 \pm 0.3$	$8.7 \pm 1.1$
	1260.5		
	1458.1		
	1678.3		
	1791.5		
$^{136}\text{Cs}$	176.7	$1.1 \pm 0.1$	$7.0 \pm 1.7$
	340.6		
	818.5		
	1048.1		
	1235.4		
* $^{139}\text{Ce}$	165.8	$1.5 \pm 0.3$	$2.4 \pm 0.2$
$^{140}\text{Ba}$	423.7	$1.1 \pm 0.2$	$5.3 \pm 0.5$
	537.3		
$^{141}\text{Ce}$	145.4	$1.2 \pm 0.1$	$7.1 \pm 0.7$

Table I

Target Fragment Recoil Properties			
4.8 GeV $^{12}\text{C} + ^{238}\text{U}$			
Nuclide	$E_{\gamma}$ (keV)	F/B	2W(F+B)
* $^{145}\text{Eu}$	893.7	$2.4 \pm 0.4$	$2.3 \pm 0.2$
* $^{146}\text{Gd}$	747.4	$5.5 \pm 1.5$	$1.8 \pm 0.3$
* $^{149}\text{Gd}$	149.7	$4.3 \pm 0.6$	$2.7 \pm 0.3$
* $^{151}\text{Tb}$	287.2	$10.7 \pm 3.5$	$1.9 \pm 0.4$
* $^{167}\text{Tm}$	207.8	$3.2 \pm 2.0$	$1.4 \pm 0.2$
$^{169}\text{Lu}$	960.3	$3.2 \pm 2.0$	$2.4 \pm 1.2$
$^{185}\text{Pt}$	197.5	$1.2 \pm 1.0$	$1.2 \pm 1.0$
$^{192}\text{Au}$	316.5	$1.1 \pm 0.2$	$6.0 \pm 1.8$
$^{198}\text{Au}$	411.8	$2.1 \pm 0.7$	$3.7 \pm 1.0$
$^{198}\text{Tl}$	411.8	$3.3 \pm 1.1$	$2.8 \pm 0.6$
* $^{209}\text{At}$	545.1	$2.1 \pm 0.6$	$2.3 \pm 0.6$

Table II

Target Fragment Recoil Properties		
5.0 GeV $^{20}\text{Ne} + ^{238}\text{U}$		
Nuclide	F/B	2W(F+B) (mg/cm <sup>2</sup> )
$^{24}\text{Na}$	9.8 ± 0.9	20.5 ± 3.1
$^{28}\text{Mg}$	5.6 ± 0.8	24.5 ± 4.9
$^{43}\text{K}$	1.9 ± 0.2	8.1 ± 1.2
$^{48}\text{Sc}$	2.4 ± 0.6	10.9 ± 3.3
$^{72}\text{As}$	2.6 ± 0.8	7.9 ± 2.8
$^{76}\text{As}$	6.1 ± 3.1	3.7 ± 2.2
$^{87}\text{Y}$	2.1 ± 0.2	7.5 ± 1.1
$^{89}\text{Zr}$	1.4 ± 0.2	8.8 ± 1.8
$^{96}\text{Tc}$	2.6 ± 0.4	8.0 ± 1.0
$^{96}\text{Nb}$	2.5 ± 0.8	8.8 ± 3.5
$^{97}\text{Zr}$	1.3 ± 0.1	7.9 ± 0.8
$^{99}\text{Mo}$	1.3 ± 0.1	9.5 ± 0.5
$^{131}\text{I}$	1.2 ± 0.1	6.6 ± 1.0
$^{133}\text{I}$	1.3 ± 0.1	8.7 ± 0.9
$^{146}\text{Gd}$	8.0 ± 2.0	9.7 ± 1.0
$^{149}\text{Gd}$	4.6 ± 1.4	3.0 ± 1.2
$^{160}\text{Er}$	1.7 ± 1.0	4.7 ± 0.5

Table III

Target Fragment Kinematic Properties as Deduced from the Two-Step Vector Model 4.8 GeV $^{12}\text{C} + ^{238}\text{U}$						
Nuclide	k	N	$\langle R \rangle$ (mg/cm $^2$ )	$\beta_{\parallel}$ (= $v_{\parallel}/c$ )	P [=AV (MeV/c)]	$\langle E \rangle$ (MeV)
$^{24}\text{Na}$	0.649	1.74	16.88	0.0203	1294	42.6
$^{28}\text{Mg}$	0.667	1.69	15.73	0.0170	1398	42.6
$^{43}\text{K}$	1.004	1.32	12.29	0.0164	1833	47.9
$^{44\text{m}}\text{Sc}$	1.238	1.18	9.86	0.0112	1635	36.9
$^{46}\text{Sc}$	1.260	1.18	11.58	0.0132	1891	47.4
$^{48}\text{Sc}$	1.282	1.18	9.21	0.00901	1564	31.0
$^{48}\text{V}$	1.388	1.12	10.23	0.0115	1754	39.1
$^{56}\text{Mn}$	1.479	1.06	7.73	0.00707	1528	25.5
$^{59}\text{Fe}$	1.458	1.07	8.38	0.00646	1702	29.0
$^{69\text{m}}\text{Zn}$	1.433	1.06	10.73	0.00550	2396	51.1
$^{71}\text{As}$	1.304	1.07	8.92	0.00788	2184	40.9
$^{72}\text{As}$	1.313	1.07	9.42	0.00401	2302	44.7
$^{74}\text{As}$	1.329	1.07	8.98	0.00591	2204	40.0
$^{76}\text{As}$	1.346	1.07	7.74	0.00526	1921	29.6
$^{77}\text{Br}$	1.281	1.08	7.55	0.00510	1949	30.1
$^{78}\text{As}$	1.363	1.07	13.74	0.00662	3278	84.5

Table III

Target Fragment Kinematic Properties as Deduced from the Two-Step Vector Model						
4.8 GeV $^{12}\text{C} + ^{238}\text{U}$						
Nuclide	k	N	$\langle R \rangle$ (mg/cm $^2$ )	$\beta_{\parallel}$ (= $V_{\parallel}/c$ )	P [=AV (MeV/c) ]	$\langle E \rangle$ (MeV)
$^{81}\text{Rb}$	1.203	1.10	8.80	0.00672	2358	41.9
$^{82}\text{Br}$	1.318	1.08	6.56	0.00105	1718	22.0
$^{82\text{m}}\text{Rb}$	1.210	1.10	6.47	0.00423	1786	23.7
$^{83}\text{Rb}$	1.216	1.10	7.83	0.00422	2126	33.3
$^{86}\text{Rb}$	1.236	1.10	7.21	0.00317	1978	27.7
$^{87\text{m}}\text{Y}$	1.129	1.13	5.79	0.00401	1701	20.3
$^{88}\text{Zr}$	1.125	1.12	5.89	0.00511	1761	21.5
$^{88}\text{Y}$	1.135	1.13	8.93	0.00537	2503	43.5
$^{89}\text{Zr}$	1.130	1.12	7.17	0.00474	2101	30.3
$^{90\text{m}}\text{Y}$	1.146	1.13	7.80	0.00553	2226	33.6
$^{90}\text{Nb}$	0.999	1.18	5.25	0.00454	1645	54.0
$^{91}\text{Sr}$	1.421	1.03	10.93	0.00242	2975	59.2
$^{92}\text{Y}$	1.157	1.13	7.84	0.00107	2239	33.3
$^{93\text{m}}\text{Mo}$	1.100	1.14	5.63	0.00348	1733	19.7
$^{95}\text{Zr}$	1.163	1.12	9.63	0.00094	2754	48.7
$^{95}\text{Nb}$	1.021	1.18	4.15	0.00161	1360	11.9

Table III

Target Fragment Kinematic Properties as Deduced from the Two-Step Vector Model						
4.8 GeV $^{12}\text{C} + ^{238}\text{U}$						
Nuclide	k	N	$\langle R \rangle$ (mg/cm $^2$ )	$\beta_{\parallel}$ (= $V_{\parallel}/c$ )	P [=AV (MeV/c) ]	$\langle E \rangle$ (MeV)
$^{95}\text{Tc}$	1.012	1.18	5.60	0.00569	1765	20.0
$^{96}\text{Nb}$	1.025	1.18	7.60	0.00172	2272	32.8
$^{96}\text{Tc}$	1.003	1.18	6.18	0.00418	1941	24.0
$^{97}\text{Ru}$	0.982	1.18	5.04	0.00406	1681	17.8
$^{97}\text{Zr}$	1.174	1.12	9.74	0.00159	2786	48.9
$^{99}\text{Mo}$	1.105	1.14	9.55	0.00197	2834	49.5
$^{101\text{m}}\text{Rh}$	0.955	1.20	5.56	0.0046	1867	21.0
$^{103}\text{Ru}$	1.006	1.18	9.21	0.00228	295	47.6
$^{105}\text{Ru}$	1.014	1.18	9.80	0.00090	3000	52.2
$^{105}\text{Rh}$	0.970	1.20	7.62	0.00383	2446	34.8
$^{106\text{m}}\text{Ag}$	0.899	1.22	5.57	0.00019	1940	21.7
$^{111}\text{In}$	0.931	1.19	4.91	0.00389	1812	18.0
$^{111\text{m}}\text{Pd}$	1.245	1.07	10.52	0.00321	3347	61.5
$^{115}\text{Cd}$	1.122	1.11	9.34	0.00189	3107	51.1
$^{115\text{m}}\text{In}$	0.944	1.19	13.42	0.00275	4241	95.5
$^{117\text{m}}\text{Sn}$	1.082	1.11	8.78	0.00380	3032	48.0

Table III

Target Fragment Kinematic Properties as Deduced from the Two-Step Vector Model						
4.8 GeV $^{12}\text{C} + ^{238}\text{U}$						
Nuclide	k	N	$\langle R \rangle$ (mg/cm $^2$ )	$\beta_{\parallel}$ (= $V_{\parallel}/c$ )	P [=AV (MeV/c)]	$\langle E \rangle$ (MeV)
$^{117}\text{Sb}$	0.858	1.23	5.30	0.00187	2027	21.4
$^{119\text{m}}\text{Te}$	0.703	1.34	4.81	0.00350	1932	19.2
$^{120}\text{Sb}$	0.867	1.23	4.37	0.00208	1739	15.4
$^{121}\text{Te}$	0.710	1.34	3.78	0.00346	1621	13.3
$^{122}\text{Sb}$	0.872	1.23	8.06	0.00205	2875	41.3
$^{124}\text{Sb}$	0.877	1.23	6.01	0.00018	2270	25.4
$^{124}\text{I}$	0.857	1.22	6.31	0.00297	2440	29.3
$^{127}\text{Sb}$	0.885	1.23	8.58	0.00016	3044	44.6
$^{130}\text{I}$	0.873	1.22	6.80	0.00179	2617	32.1
$^{131}\text{Ba}$	0.626	1.40	4.14	0.00341	1863	16.1
$^{131}\text{I}$	0.875	1.22	8.41	0.00137	3120	45.4
$^{132}\text{Te}$	0.728	1.34	7.15	0.00046	2665	32.9
$^{132}\text{Cs}$	0.780	1.27	5.59	0.00229	2295	24.3
$^{132}\text{I}$	0.878	1.22	5.29	0.00118	2135	21.1
$^{133}\text{I}$	0.881	1.22	8.78	0.00038	3240	48.1
$^{135}\text{Xe}$	0.948	1.18	8.20	0.00109	3087	43.1

Table III

Target Fragment Kinematic Properties as Deduced from the Two-Step Vector Model						
4.8 GeV $^{12}\text{C} + ^{238}\text{U}$						
Nuclide	k	N	$\langle R \rangle$ (mg/cm $^2$ )	$\beta_{\parallel}$ (= $V_{\parallel}/c$ )	P [=AV (MeV/c) ]	$\langle E \rangle$ (MeV)
$^{135}\text{I}$	0.886	1.22	8.64	0.00196	3207	46.5
$^{136}\text{Cs}$	0.788	1.27	6.95	0.00032	2737	33.7
$^{139}\text{Ce}$	0.478	1.54	2.37	0.00099	1389	8.4
$^{140}\text{Ba}$	0.630	1.40	5.28	0.00047	2259	22.3
$^{141}\text{Ce}$	0.480	1.54	7.05	0.00076	2825	34.6
$^{145}\text{Eu}$	0.308	1.89	2.16	0.00142	1382	8.0
$^{146}\text{Gd}$	0.294	1.90	1.44	0.00302	1138	5.4
$^{149}\text{Gd}$	0.295	1.90	2.28	0.00327	1461	8.7
$^{151}\text{Tb}$	0.286	1.92	1.29	0.00388	1099	4.9
$^{167}\text{Tm}$	0.237	2.05	1.25	0.00184	1179	5.1
$^{169}\text{Lu}$	0.261	1.91	2.15	0.00252	1595	9.2
$^{185}\text{Pt}$	0.193	2.09	1.23	0.0029	1335	5.9
$^{192}\text{Au}$	0.389	1.53	5.96	0.0048	3438	37.6
$^{198}\text{Au}$	0.392	1.53	3.48	0.00229	2442	18.4
$^{198}\text{Tl}$	0.227	1.90	2.47	0.00279	2020	12.5
$^{209}\text{At}$	0.198	1.97	2.19	0.00161	1992	11.6

Table IV

Target Fragment Kinematic Properties As Deduced from the Two Step Vector Model (5.0 GeV Ne + $^{238}\text{U}$ )			
Nuclide	$\beta_{\parallel}$ (= $V_{\parallel}/c$ )	P [=AV (MeV/c) ]	<E> (MeV)
$^{24}\text{Na}$	0.025	1294	42.4
$^{28}\text{Mg}$	0.023	1705	63.8
$^{43}\text{K}$	0.0049	1231	21.7
$^{48}\text{Sc}$	0.0083	1740	38.3
$^{72}\text{As}$	0.0084	1820	28.1
$^{76}\text{As}$	0.0050	856	5.9
$^{87}\text{Y}$	0.0045	2013	28.7
$^{96}\text{Nb}$	0.0061	2397	36.8
$^{96}\text{Tc}$	0.0059	2280	32.6
$^{97}\text{Zr}$	0.00161	2245	31.9
$^{99}\text{Mo}$	0.0020	2774	47.7
$^{131}\text{I}$	0.00088	2474	28.4
$^{133}\text{I}$	0.0016	3119	44.8
$^{146}\text{Gd}$	0.011	3157	41.4
$^{149}\text{Gd}$	0.020	3494	50.1
$^{160}\text{Er}$	0.0019	2388	21.5

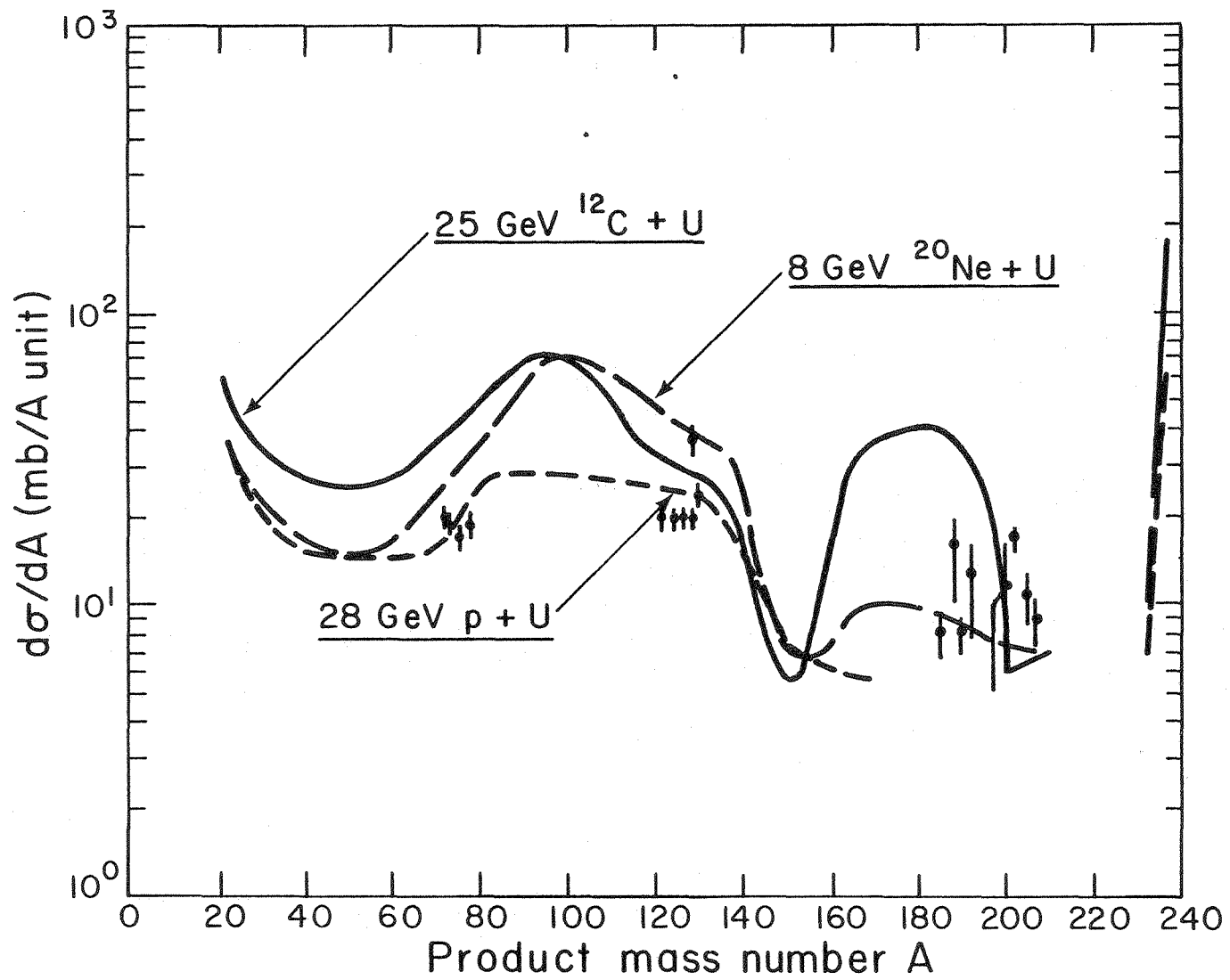


Fig. 1

XBL 794-1255A

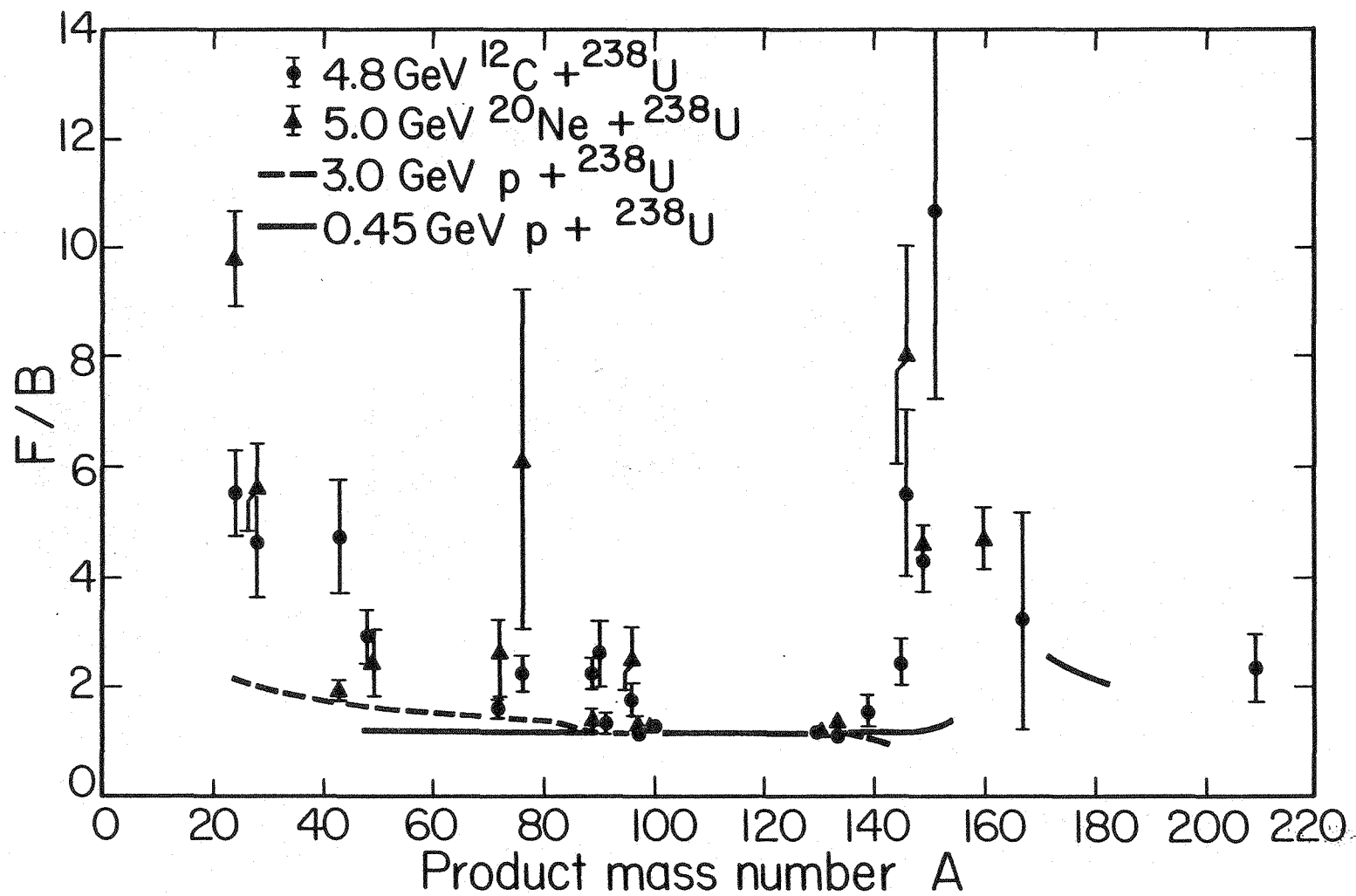


Fig. 2

XBL 808-1741

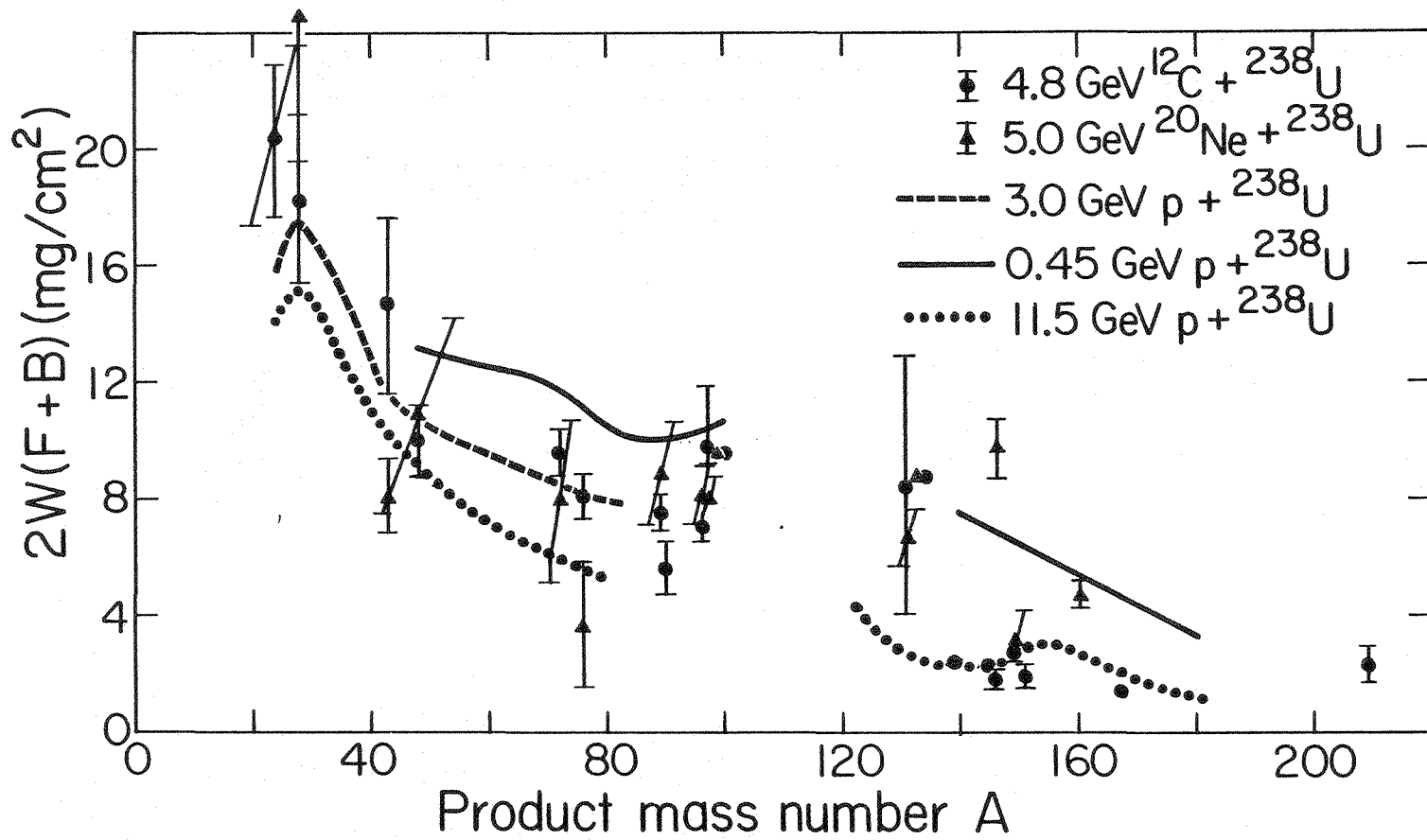


Fig. 3

XBL 808-1740

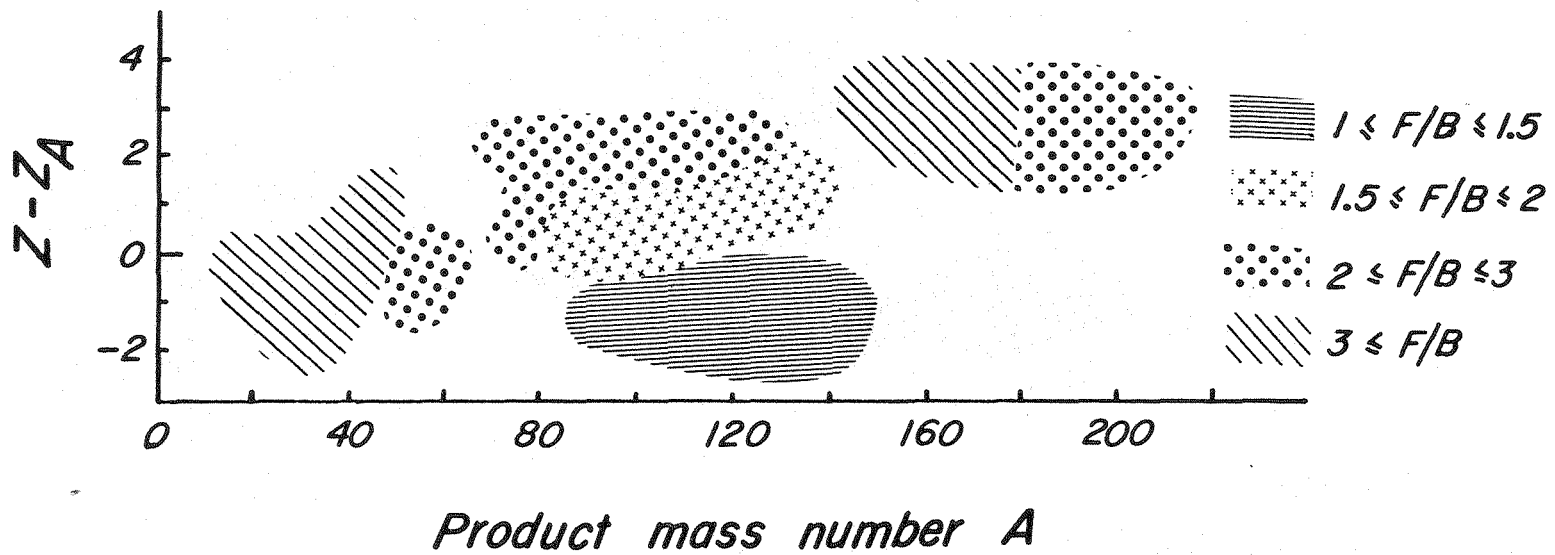


Fig. 4

XBL 8010-12264

**Target Fragment Energies**

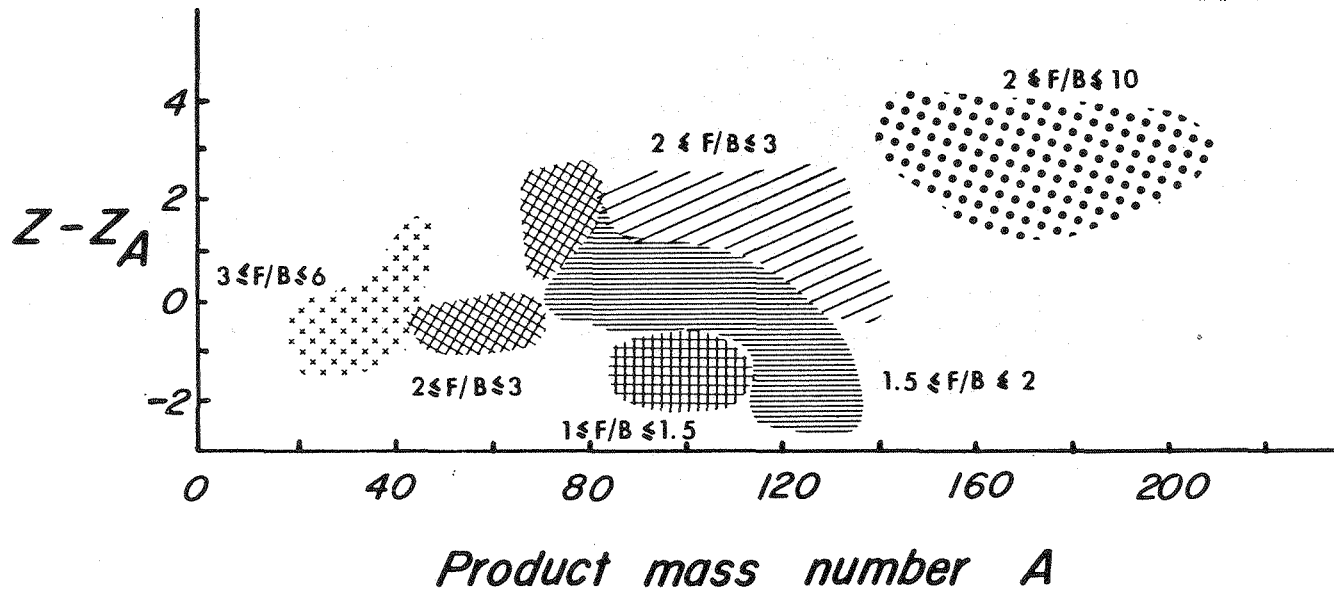
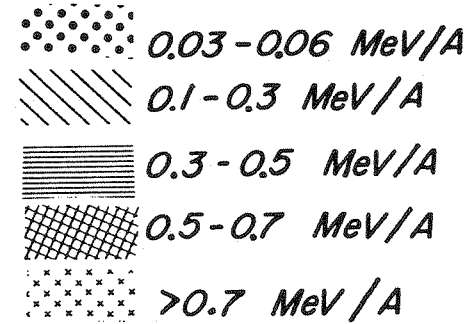
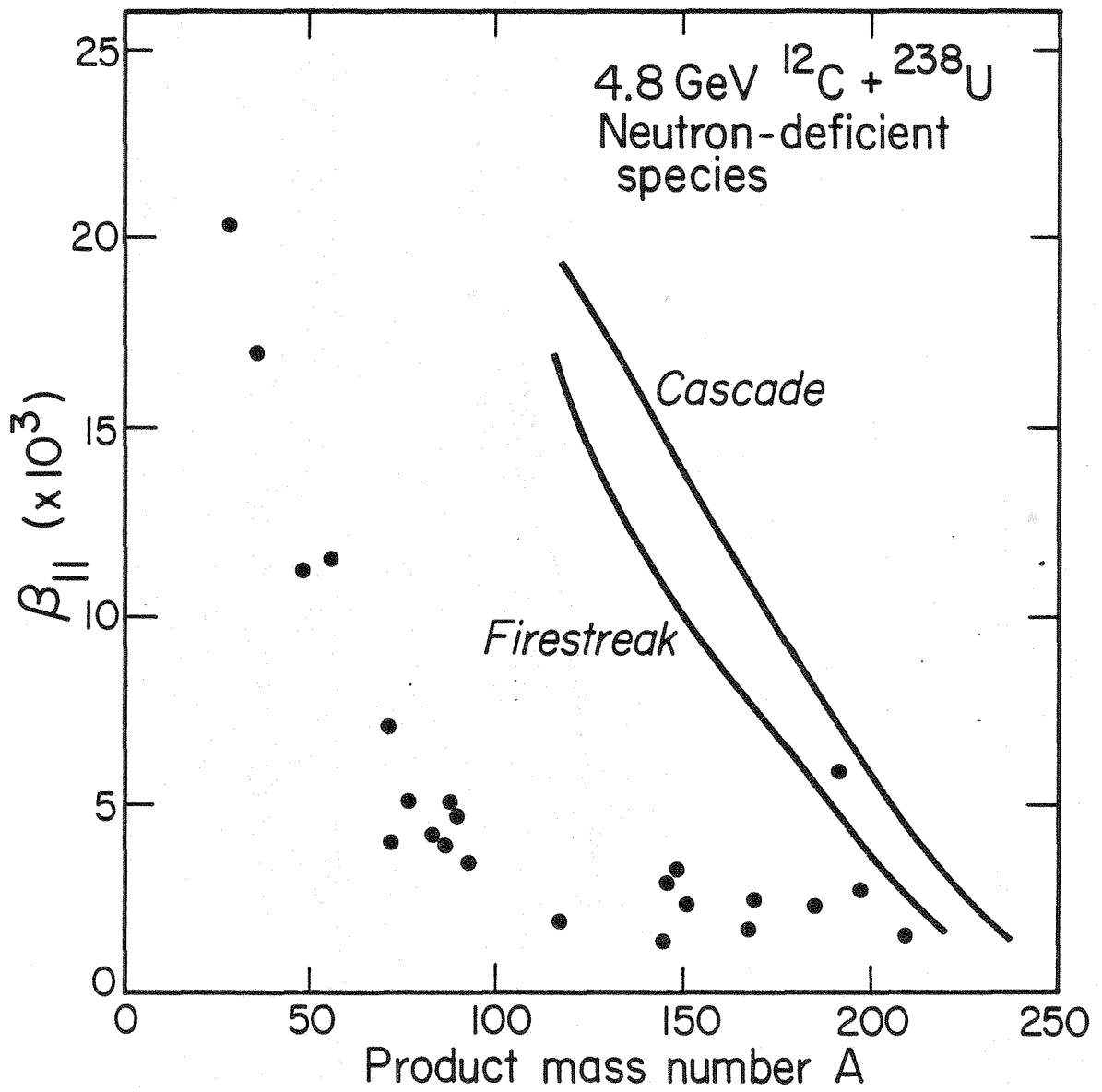


Fig. 5



XBL 808-1743

Fig. 7

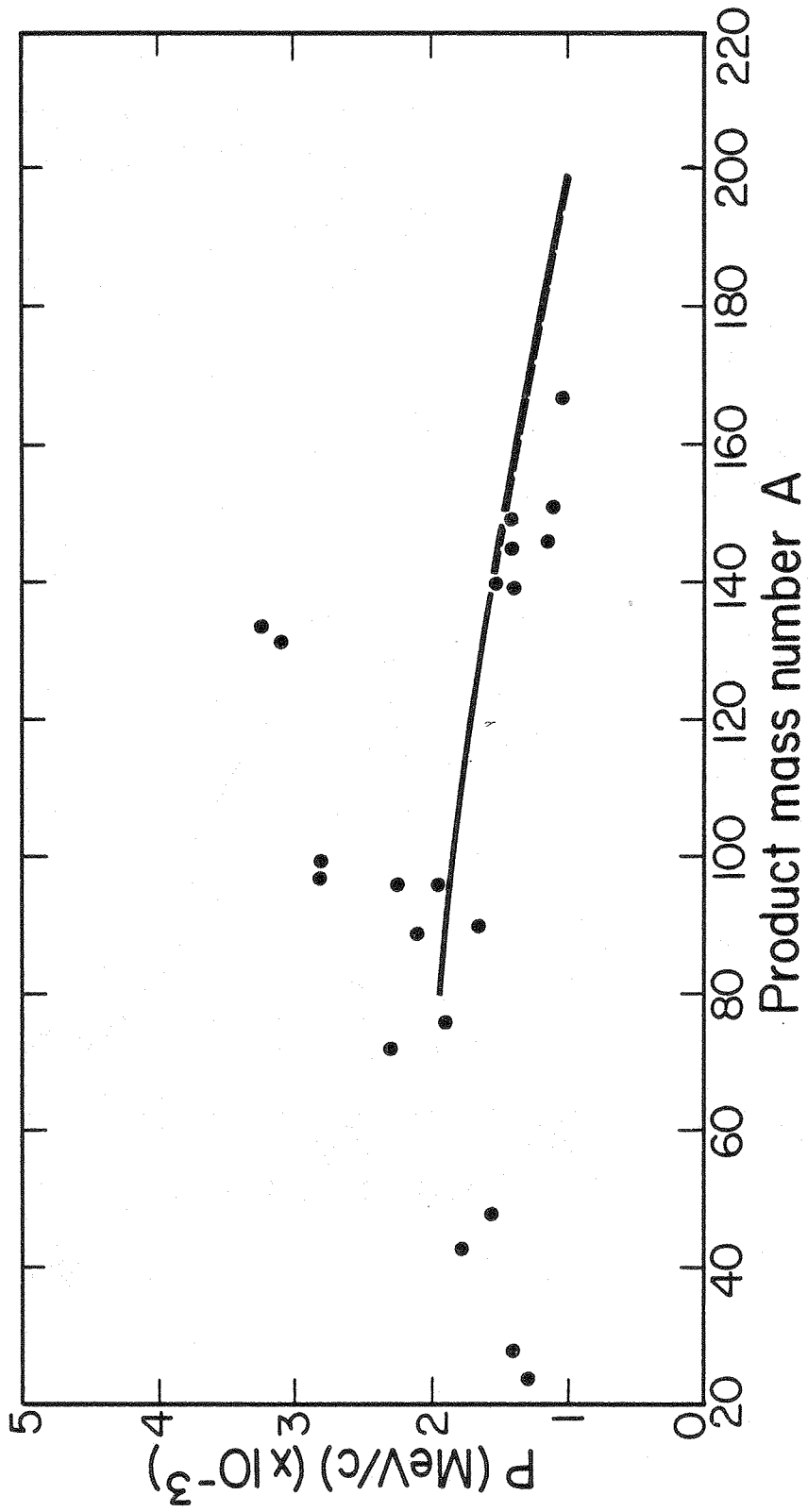


Fig. 6

XBL 808-1742